J Mol Model (2013) 19:1763–1777
DOI 10.1007/s00894-012-1716-5

ORIGINAL PAPER

Microsolvation of Mg^{2+}, Ca^{2+}: strong influence of formal charges in hydrogen bond networks

Juan David Gonzalez · Elizabeth Florez · Jonathan Romero · Andrés Reyes · Albeiro Restrepo

Received: 15 October 2012 / Accepted: 27 November 2012 / Published online: 10 January 2013

Abstract A stochastic exploration of the quantum conformational spaces in the microsolvation of divalent cations with explicit consideration of up to six solvent molecules $[Mg(H_2O)_n)]^{2+}$, (n=3, 4, 5, 6) at the B3LYP, MP2, CCSD(T) levels is presented. We find several cases in which the formal charge in Mg^{2+} causes dissociation of water molecules in the first solvation shell, leaving a hydroxide ion available to interact with the central cation, the released proton being transferred to outer solvation shells in a Grotthus type mechanism; this particular finding sheds light on the capacity of Mg^{2+} to promote formation of hydroxide anions, a process necessary to regulate proton transfer in enzymes with exonuclease activity. Two distinct types of hydrogen bonds, scattered over a wide range of distances (1.35–2.15 Å) were identified. We find that in inner solvation shells, where hydrogen bond networks are severely disturbed, most of the interaction energies come from electrostatic and polarization+charge transfer, while in outer solvation shells the situation approximates that of pure water clusters.

Keywords Hydrogen bonding · Microsolvation of cations · Stochastic optimization

Electronic supplementary material The online version of this article (doi:10.1007/s00894-012-1716-5) contains supplementary material, which is available to authorized users.

J. D. Gonzalez · A. Restrepo (✉)
Instituto de Química, Universidad de Antioquia,
AA 1226, Medellín, Colombia
e-mail: albeiro@matematicas.udea.edu.co

E. Florez
Departamento de Ciencias Básicas,
Universidad de Medellín, Medellín, Colombia

J. Romero · A. Reyes
Departamento de Química, Universidad Nacional de Colombia,
Av. Cra. 30 #45-03,
Bogota, Colombia

Introduction

The study of solvated metal cations, $[M\ (H_2O)_n]^{q+}$, with M=alkali, alkali earth or transition metal ions has attracted considerable attention [1–6]. Among these clusters, calcium and magnesium hydrated ions have been intensively studied due to the important roles they play in biochemical functions of the human body [8–10]. For example, Mg^{2+} stabilizes the three dimensional structure of many functional RNA molecules; Ca^{2+} is involved in signal transduction, blood clotting, muscle contraction, cell division, and many other biological processes [7].

Of particular interest is the study of partial hydration of divalent cations in enzymes. A large number of X–ray diffraction experiments have shown that in many of the magnesium–dependent enzymes, the Mg^{2+} cation always appears partially hydrated [8–10]. The number of water molecules in the first solvation shell of Mg^{2+} in proteins ranges from one to six, with rare cases of up to seven molecules being found in the Protein Data Bank (PDB). The presence of these water molecules is essential for a large number of enzymatic pathways occurring through interactions between protein residues and water molecules bonded to Mg^{2+} (outer–sphere binding) [9, 10].

One process where hydrated divalent cations play an important role is exonuclease activity. The classical example is RNA hydrolysis, in which the deprotonation of a metal–bonded water molecule promotes phosphodiester bond breaking by aiding in the departure of the leaving group [11–15]. In most cases, Mg^{2+} serves as a cofactor of exonucleases. Although other divalent metal ions may also activate enzymes with exonuclease activity, this is frequently accompanied by a reduction of enzyme efficiency and/or substrate specificity [10]. Understanding Mg^{2+} hydration and the comparative differences with respect to microsolvation of other divalent cations, such as Ca^{2+}, is essential to rationalize differences in their biological roles.

Several experimental and theoretical methods [16–21] have been used to study the structure of solvated Mg^{2+} and Ca^{2+}. Even though both are divalent ions, they interact with water in different ways because of their different sizes and electron configurations. Experimentally, it has been found that Mg^{2+} binds six water molecules in an octahedral orientation [22], whereas the coordination number of Ca^{2+} reported from various X–Ray neutron diffraction and EXAFS experiments varies from 6 to 10 [23–25]. One particular work, very relevant to our case, found no evidence of hydrogen bonding within $[Ca\ (H_2O)_n]^{2+}$ clusters for $n \leq 6$, therefore, for those cluster sizes, at the experimental conditions, all water molecules are seen to coordinate exclusively with the central cation [26].

On the theoretical side, solvated Mg^{2+} and Ca^{2+} have been studied at different levels of theory. Lightstone and coworkers [27] employed molecular dynamics (MD) techniques to find that the first solvation shell around Mg^{2+} contains six water molecules. Similarly, Markham et al. [28], employing ab initio methods, have reported that $[Mg\ (H_2O)_5]^{2+}$, $[Mg\ (H_2O)_6]^{2+}$ clusters lead to more stable structures by directly coordinating all water molecules to the central cation instead of distributing them among two solvation shells. In the case of solvated Ca^{2+}, it has been found through MD and ab initio methods that the coordination number varies between 7.0 and 9.2 [29–31]. On the other hand, DFT simulations have predicted that the highest stability of hydrated Ca^{2+} is achieved when surrounded by six water molecules [3, 19, 23, 32], whereas the second shell might be fully occupied with varying numbers of solvent molecules. The same study suggests that at finite temperatures, the lowest energy conformations (global minima) coexist with metastable isomers (local minima) for a given cluster size. This finding is very much in agreement with a popular view of the structure of liquids held together via hydrogen bond networks; according to this view, liquid water for example [33], is considered not to be an isotropic medium, showing local fluctuations in both the structure and size of contributing water microclusters.

Previous studies on the microsolvation of cations mainly focus on the geometries, binding energies, and on the disposition of water molecules in the first and second hydration shells. An important issue is to investigate the nature and interplay among the different types of stabilizing interactions present in $[Mg\ (H_2O)_n]^{2+}$ and in $[Ca\ (H_2O)_n]^{2+}$. Sastry and coworkers [34, 35] have shown that polarization and charge transfer are major players in the interaction energies between both isolated and solvated cations ↔ π–systems. Of particular interest is the magnified "enhancing" effect [5, 6] of the +2 formal charge on the central cation and its influence on the arrangement of the neighboring water molecules.

A sensitive issue in the study of atomic and molecular clusters is the generation of equilibrium structures. A recent modification of the Metropolis acceptance test during the simulated annealing optimization procedure has been implemented into the ASCEC program [36–38]. ASCEC (after its Spanish acronym Annealing Simulado Con Energía Cuántica) simulations generate cluster candidate structures that undergo further optimization by traditional gradient following techniques. The method retains the comparative advantages and disadvantages of stochastic optimization over analytical methods, namely, initial guess independence, exhaustive exploration of the potential energy surface, and the ability to jump over energy barriers and to sample several energy wells on the same run without getting trapped in local minima; the method is still computationally intensive because of repetitive evaluation of the quantum energy function. Successful application of the ASCEC methodology has allowed the treatment of systems stabilized via a wide variety of complex interactions; cases of study have been mono– and bi–metallic atomic microclusters [37, 39, 40], molecular clusters joint via hydrogen bonding networks [36, 41–45] and in a closely related study to the subject of this report, mixed monovalent cation/water clusters [4] (specifically $[Li(H_2O)_n]^+$). The studies in question afforded contributing new structures never before reported in the literature, which in the proper cases have helped in rationalizing the stabilization of small hydrogen–bonded networks, the reactivity of metallic microclusters and the nature and complex competition between several interactions in the microsolvation of alkali metal cations.

In this work, a stochastic exploration of the HF/6–31G* potential energy surfaces (PESs) to produce candidate cluster structures for $[Mg(H_2O)_n]^{2+}$ and $[Ca(H_2O)_n]^{2+}$, (n=3, 4, 5, 6) was performed using the ASCEC program; the candidate structures are further optimized and characterized by means of DFT and second order perturbation theory at the B3LYP/6–31G* and MP2/6–311++G** levels. Highly correlated CCSD (T)/6–311++G** energies were calculated on all MP2 optimized geometries. Energy decomposition analysis (EDA) was carried out in order to gain insight into the interactions responsible for cluster stabilization. We aim at expanding the limited knowledge of these very important PESs and to contribute to the understanding of the nature and roles of the several interactions at play in stabilizing the clusters.

Computational methods

We used the big bang approach to construct the initial geometries for all ASCEC runs. In this method, the metal atom together with all water molecules are placed at the center of a cubic box and allowed to evolve as overall divalent cationic systems under the annealing conditions. Duplicate runs were calculated with the same sets of parameters for every PES. The systems were placed inside cubic

boxes of lengths varying from 6 to 9 Å according to the number of water molecules. The HF/6–31G* model chemistry was used to calculate the energy of randomly generated Markov chains of cluster configurations. Geometrical quenching routes with initial temperatures of 500 K, 5 % decrease in temperature and 100 total temperatures were used, with this plan, simulations run down to 2.96 K.

All optimization, frequency and energy calculations in this work were carried out using the Gaussian 09 suite of programs [46]. Characterization of stationary points as true minima or saddle points was carried out by counting the number of negative eigenvalues of the Hessian matrix resulting from analytical harmonic second order derivative calculations at the same optimization levels. Highly correlated CCSD(T)/6–311++G** energies were computed on all MP2 optimized geometries. Total binding energies (ΔE_B) were calculated by subtracting the energy of a given cluster from the sum of the energies of its constituting moieties. We calculated relative binding energies ($\Delta\Delta E_B$) as the difference between the energy of the most stable structure and the energy of a particular cluster on a given PES. Energy decomposition analysis (EDA) calculations proposed by Su and Li [47] were performed using the GAMESS 2010 software package [48] with an MP2/6–311++G** method. Calculations were performed on the structures optimized at the same level of theory. Lei and Pan [3] found negligible contributions to binding energies when the basis set superposition error was accounted for in their study of microsolvated Ca^{2+} with explicit consideration of 1–20, 27 water molecules, therefore we restrain ourselves from applying such methods in this work.

Results and discussion

Geometrical and structural issues

Our calculations produced equilibrium geometries for the $[Mg(H_2O)_n]^{2+}$, $[Ca(H_2O)_n]^{2+}$ (n=3, 4, 5, 6) clusters following the procedure outlined above. The geometrical motifs and notation within each PES are shown in Figs. 1, 2, 3 and 4. Strictly speaking, all geometries belong to the C_1 point group as the structures are randomly generated and further optimized without imposition of symmetry constraints, however, some of the located stationary points have approximate higher effective symmetries (concerning heavy atoms only). A few structures exhibit one imaginary frequency at the MP2 level while being well defined minima at the B3LYP level. We discuss next the 66 structures found in this work.

$[M(H_2O)_3]^{2+}$ clusters

Figure 1 shows the six stable motifs found when three water molecules surround the title cations. W_3S_1, W_3S_3, W_3S_5, and W_3S_6, are found for Mg^{2+} while structures W_3S_1, W_3S_2, W_3S_4, and W_3S_6 are found for Ca^{2+}. For both cations, the most stable structures, according to CCSD(T) calculations (Tables 1 and 2) exhibit approximate heavy–atom D_{3h} symmetry. All structures, with the exception of W_3S_1, the most stable one, exhibit a second solvation shell. In the W_3S_5 structure, only appearing on the $[Mg(H_2O)_3]^{2+}$ surface, the strong influence of the formal +2 charge in Mg leads to dissociation of one water molecule, leaving a hydroxide anion which strongly binds to magnesium, while the remaining proton produced by water breakage transfers to a water molecule in the second solvation shell, which in turn produces a Zundel type cation between the excess proton and two water molecules in the second and third solvation shells; the entire proton transfer process being reminiscent of the well known mechanism proposed by Grotthus in 1806 [49]. Similar structures with dissociated water molecules are seen in other PESs for the microsolvation of Mg^{2+} with larger numbers of water molecules. Comparison between W_3S_5 and W_3S_6, structures for which magnesium coordination number is one, suggests that the structures of water networks surrounding Mg^{2+} change as a function of the type of hydrogen bonding.

$[M(H_2O)_4]^{2+}$ clusters

Stable cluster conformations are shown in Fig. 2. W_4S_9 appears on the $[Mg(H_2O)_4]^{2+}$ PES only, while W_4S_2, W_4S_5, and W_4S_8 are present only on the $[Ca(H_2O)_4]^{2+}$ PES, all other motifs are common to both surfaces. In both cases, CCSD(T) calculations (Table 1 and 2) predict a structure with approximate S_4 symmetry to be the global minimum (approximate T_d if the H atoms are not considered). Interestingly, W_4S_2 is very close in energy to W_4S_1 for the Ca^{2+} case, however, it is not present on the microsolvation of Mg^{2+}. We point out that second and third solvation shells are not present on the most stable structures. For Mg^{2+}, W_4S_9 shows one dissociated water molecule in the first solvation shell which leads to a Zundel type cation involving water molecules in the second and third solvation shells.

$[M(H_2O)_5]^{2+}$ clusters

When 5 water molecules surround Mg^{2+} and Ca^{2+}, the most stable structures are predicted to have all waters directly coordinated to the central cation (Tables 1 and 2, Fig. 3). Exclusive to $[Mg(H_2O)_5]^{2+}$ are structures W_5S_6, W_5S_8, W_5S_{11}, W_5S_{12}, while W_5S_4, W_5S_9, W_5S_{10}, are only present on the $[Ca(H_2O)_5]^{2+}$ PES, all other motifs in Fig. 3 are common to both cations. Structures with up to four solvation shells are observed in the least stable conformations. For Mg^{2+}, W_5S_8, W_5S_{11}, W_5S_{12}, show dissociated water molecules leading to Zundel type cations.

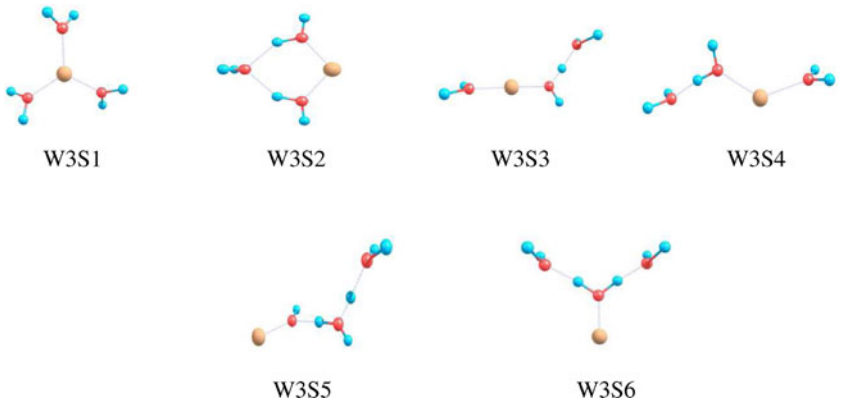

Fig. 1 Local minima on the MP2/6–311++G** PESs of $[M(H_2O)_3]^{2+}$ (M=Mg, Ca). Water dissociation in the first solvation shell produces a Zundel type cation shared between the second and third solvation shells for $[Mg(H_2O)_3]^{2+}$ in W_3S_5 via a Grotthus mechanism. Lines joining atoms are drawn to help visualization of the geometrical motifs

$[M(H_2O)_6]^{2+}$ clusters

Octahedral arrangements of six oxygen atoms around the central atom are observed in the most stable structures for both cations, as has been reported in experimental works for $[Mg(H_2O)_6]^{2+}$ clusters [22]. Interestingly, as opposed to the cases of microsolvation with fewer water molecules (Mg^{2+}, Ca^{2+}), the smaller coordination number for the central cation in the $[M(H_2O)_6]^{2+}$ clusters is 3: no structure is predicted to have only one or two waters directly coordinated to the central cation when a total of six water molecules are considered; as a consequence, the largest number of solvation shells in our structures is three. For Mg^{2+}, W_6S_{15} shows one dissociated water leading to a Zundel type cation.

All PESs for the microsolvation of Mg^{2+} exhibit at least one local minima for which one dissociated water molecule exists, leading to Zundel type cations, interestingly, no Eigen type cations are seen for any number of waters considered in this study for the microsolvation of Mg^{2+}, Ca^{2+}.

Structural differences between hydrated Ca^{+2} and Mg^{+2}

Distribution plots for metal···oxygen and for hydrogen bond distances calculated at the MP2/6–311++G** level are presented in Fig. 5. Clear differences are observed for microsolvation of Mg^{2+} and Ca^{2+}:

(i) For the *same* geometrical motifs, Mg···O distances are considerably smaller than Ca···O distances, the former distributing in a Gaussian–like fashion over the 1.85–2.15 Å range centered around 2.00 Å, the latter covering the 2.15–2.40 Å range, peaking at about 2.40 Å. These results are in agreement with theoretical and experimental distances previously reported [17–21]. It is very interesting that for Mg^{2+}, the distribution of metal···oxygen distances is centered around a well defined value, while it is non symmetric for Ca^{2+}. This observation suggests that there are different dominant interactions for each system, given that Mg···O distances allow more flexibility than Ca···O distances.

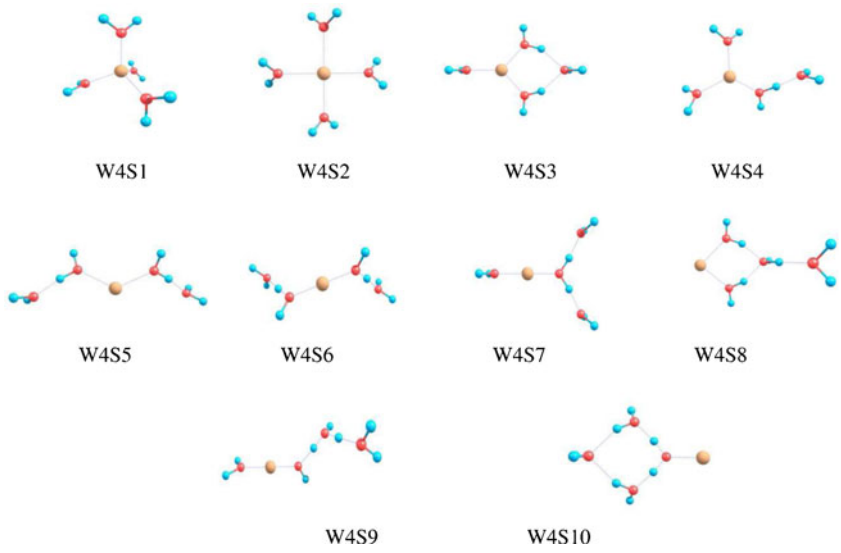

Fig. 2 Local minima on the MP2/6–311++G** PESs of $[M(H_2O)_4]^{2+}$ (M=Mg, Ca). Water dissociation produces a Zundel type cation for $[Mg(H_2O)_3]^{2+}$ in W_4S_9. Lines joining atoms are drawn to help visualization of the geometrical motifs

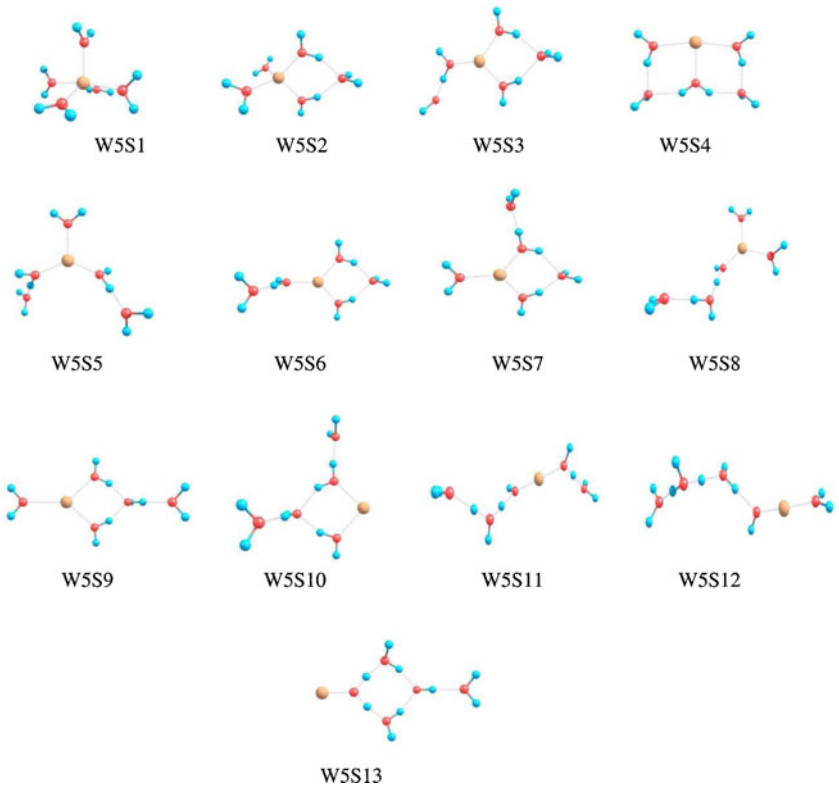

Fig. 3 Local minima on the MP2/6–311++G** PESs of $[M(H_2O)_5]^{2+}$ (M=Mg, Ca). Water dissociation produces Zundel type cations for $[Mg(H_2O)_3]^{2+}$ in W_5S_8, W_5S_{11} and W_5S_{12}. Lines joining atoms are drawn to help visualization of the geometrical motifs

(ii) Two distinct types of hydrogen bonds are observed: regular 1 donor →1 acceptor H–bonds and 2 donors →1 acceptor H–bonds, such as those present for example in structure W_3S_2. Similar intensity patters are observed for

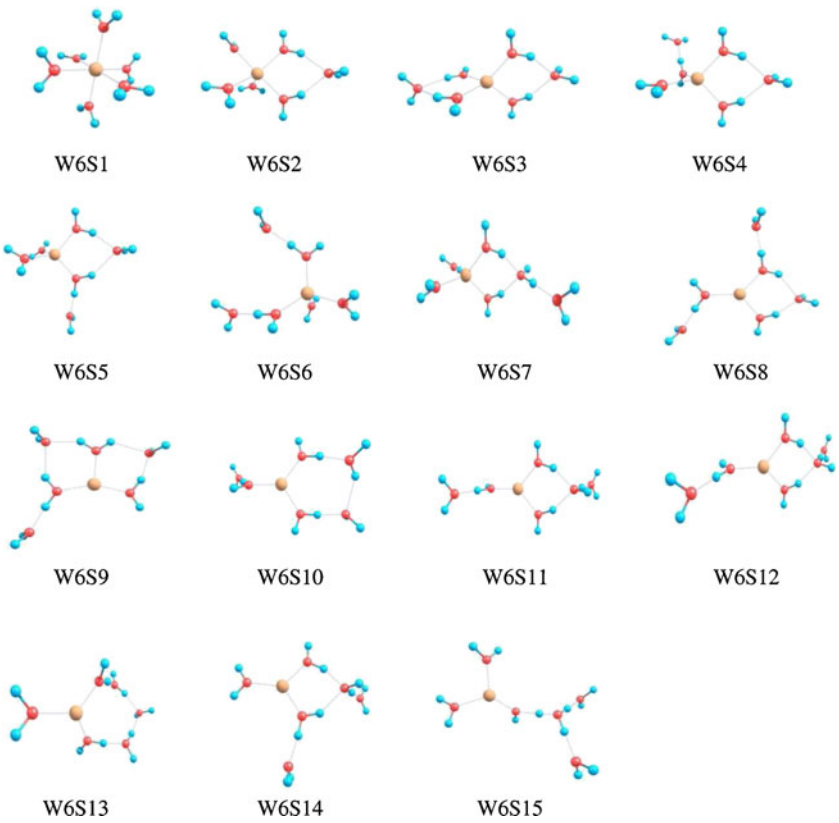

Fig. 4 Local minima on the MP2/6–311++G** PESs of $[M(H_2O)_6]^{2+}$ (M=Mg, Ca). Water dissociation produces a Zundel type cation for $[Mg(H_2O)_3]^{2+}$ in W_6S_{15}. Lines joining atoms are drawn to help visualization of the geometrical motifs

Table 1 $[Mg(H_2O)_n]^{2+}$ total (ΔE_B) and relative ($\Delta\Delta E_B$) binding energies calculated at the B3LYP/6–31G*, MP2/6–311++G** and CCSD(T)/6–311++G**//MP2/6–311++G** levels of theory. All energies (in kcal mol^{-1}) were corrected for the corresponding unscaled zero–point energies (ZPE). *m* is the coordination number of the central cation. Heavy–atom symmetries are only approximate, strictly speaking, all structures belong to the C_1 group (see text)

Structure	Heavy–atom symmetry	ΔE_B B3LYP	ΔE_B MP2	ΔE_B CCSD(T)	$\Delta\Delta E_B$ B3LYP	$\Delta\Delta E_B$ MP2	$\Delta\Delta E_B$ CCSD(T)	*m*
$[Mg(H_2O)_3]^{2+}$								
W_3S_1	D_{3h}	–211.02	–202.84	–202.31	0.00	0.00	0.00	3
W_3S_3	C_s	–187.92	–178.98	–177.82	23.10	23.86	24.49	2
W_3S_5	C_1	–153.43	–142.85	–141.19	57.59	60.00	60.12	1
W_3S_6	C_{2v}	–149.45	–140.50	–139.13	61.57	62.33	63.19	1
$[Mg(H_2O)_4]^{2+}$								
W_4S_1	T_d	–256.64	–249.45	–249.16	0.00	0.00	0.00	4
W_4S_3	C_{2v}	–240.28	–230.74	–230.00	16.36	18.71	19.17	3
W_4S_4	C_1	–239.75	–230.60	–229.65	16.92	18.85	19.51	3
W_4S_6	C_2	–219.06	–208.95	–207.32	37.58	40.50	41.84	2
W_4S_7	C_{2v}	–213.30	–203.70	–202.37	43.34	45.75	46.78	2
W_4S_9	C_1	–213.32	–202.79	–201.05	43.32	46.65	48.11	2
W_4S_{10}	C_s	–168.86	–158.56	–156.87	87.78	90.89	92.29	1
$[Mg(H_2O)_5]^{2+}$								
W_5S_1	C_{2v}	–286.51	–282.43	–282.50	0.00	0.00	0.00	5
W_5S_2	C_2	–283.34	–275.17	–274.78	3.18	7.24	7.82	4
W_5S_3	C_s	–267.77	–257.45	–256.59	18.75	24.97	25.91	3
W_5S_5	C_2	–266.28	–257.34	–255.05	20.24	26.08	27.45	3
W_5S_6	C_s	–267.74	–257.47	–256.33	18.77	24.95	26.17	3
W_5S_7	C_s	–266.53	–255.71	–254.63	20.98	26.71	27.87	3
W_5S_8	C_1	–260.50	–250.70	–249.12	26.01	31.72	33.38	3
W_5S_{11}	C_1	–241.87	–230.43	–228.20	44.64	51.99	54.30	2
W_5S_{12}	C_1	–234.83	–223.26	–221.31	51.69	59.15	61.19	2
W_5S_{13}	C_s	–187.01	–175.28	–173.13	99.50	107.14	109.37	1
$[Mg(H_2O)_6]^{2+}$								
W_6S_1	T_h	–313.70	–313.97	–314.47	0.00	0.00	0.00	6
W_6S_2	C_1	–311.58	–306.85	–306.75	2.12	7.12	7.72	5
W_6S_3	D_{2d}	–309.19	–300.32	–299.62	4.50	13.64	14.85	4
W_6S_4	C_1	–306.74	–297.26	–296.49	6.96	16.70	17.98	4
W_6S_5	C_1	–305.32	–297.02	–296.33	8.38	16.95	18.14	4
W_6S_6	C_1	–304.46	–296.32	–295.48	9.24	17.75	18.99	4
W_6S_7	C_1	–303.05	–293.98	–293.09	10.65	19.99	21.38	4
W_6S_8	C_s	–289.16	–280.80	–279.40	24.53	33.17	35.07	3
W_6S_9	C_s	–289.71	–277.90	–276.76	23.99	36.06	37.71	3
W_6S_{10}	C_1	–289.16	–276.98	–275.53	24.53	36.98	38.94	3
W_6S_{11}	C_s	–284.95	–276.85	–275.31	28.75	37.11	39.17	3
W_6S_{12}	C_s	–288.21	–276.84	–275.29	25.49	37.12	39.18	3
W_6S_{13}	C_2	–285.03	–274.43	–272.99	28.67	39.53	41.48	3
W_6S_{14}	C_1	–284.86	–274.00	–272.58	28.83	39.97	41.89	3
W_6S_{15}	C_1	–279.69	–268.90	–267.18	34.01	45.07	47.29	3

clusters with Mg^{+2} and Ca^{+2}, indicating that most of the H–bond motifs are common. However, there is a larger number of peaks for the former cation, suggesting that the charge in Mg^{2+} induces larger structural changes in the surrounding H–bonding network of solvent molecules. Considerable differences in distances are also observed in the hydrogen bond networks surrounding the first solvation shells for both cations.

Effects of the formal +2 charge on the hydrogen bonds

The effects of the charges in Mg^{2+}, Ca^{2+} on the interactions between the surrounding water molecules can be summarized as follows:

(i) Uncommonly short and long distances are predicted for H–bonds ($HOH\cdots OH_2$) in Mg^{2+} clusters (1.35–2.20 Å),

Table 2 $[Ca(H_2O)_n]^{2+}$ total (ΔE_B) and relative ($\Delta\Delta E_B$) binding energies calculated at the B3LYP/6–31G*, MP2/6–311++G** and CCSD(T)/6–311++G**//MP2/6–311++G** levels of theory. All energies (in kcal mol^{-1}) were corrected for the corresponding unscaled zero–point energies (ZPE). *m* is the coordination number of the central cation. Heavy–atom symmetries are only approximate, strictly speaking, all structures belong to the C_1 group (see text)

Structure	Heavy–atom symmetry	ΔE_B B3LYP	ΔE_B MP2	ΔE_B CCSD(T)	$\Delta\Delta E_B$ B3LYP	$\Delta\Delta E_B$ MP2	$\Delta\Delta E_B$ CCSD(T)	*m*
$[Ca(H_2O)_3]^{2+}$								
W_3S_1	D_{3h}	–141.80	–144.42	–143.19	0.00	0.00	0.00	3
W_3S_2	C_{2v}	–125.61	–127.91	–126.64	16.19	16.51	16.54	2
W_3S_4	C_s	–125.86	–127.85	–125.93	15.96	17.05	17.25	2
W_3S_6	C_{2v}	–103.56	–105.85	–104.39	38.24	38.58	38.80	1
$[Ca(H_2O)_4]^{2+}$								
W_4S_1	T_d	–178.36	–182.35	–180.97	0.00	0.00	0.00	4
W_4S_2	D_2	–175.17	–179.20	–177.89	3.18	3.15	3.08	4
W_4S_3	C_{2v}	–166.84	–169.06	–167.57	11.51	13.28	13.40	3
W_4S_4	C_1	–165.22	–167.74	–166.10	13.13	14.61	14.87	3
W_4S_5	C_2	–150.52	–151.74	–149.87	27.84	30.60	31.10	2
W_4S_6	C_2	–150.57	–150.20	–148.34	27.78	32.15	32.63	2
W_4S_7	C_{2v}	–147.09	–148.36	–146.71	31.27	33.98	34.26	2
W_4S_8	C_s	–145.93	–147.68	–145.95	32.43	34.65	35.02	2
W_4S_{10}	C_s	–119.12	–121.67	–119.94	59.23	60.67	61.03	1
$[Ca(H_2O)_5]^{2+}$								
W_5S_1	C_{2v}	–207.45	–213.53	–212.21	0.00	0.00	0.00	5
W_5S_2	C_2	–201.93	–205.48	–203.88	5.52	8.04	8.33	4
W_5S_3	C_s	–189.56	–191.44	–189.56	17.89	22.09	22.66	3
W_5S_4	C_{2v}	–188.38	–190.33	–189.28	19.07	22.59	22.93	3
W_5S_7	C_s	–187.62	–190.09	–188.30	19.82	23.44	23.91	3
W_5S_5	C_2	–187.72	–189.76	–187.78	19.72	23.77	24.43	3
W_5S_9	C_s	–189.59	–187.67	–185.73	17.85	25.86	26.48	3
W_5S_{10}	C_1	–166.83	–168.98	–166.99	40.62	44.54	45.22	2
W_5S_{13}	C_s	–134.55	–136.68	–134.54	72.90	76.84	77.67	1
$[Ca(H_2O)_6]^{2+}$								
W_6S_1	T_h	–233.94	–242.64	–241.48	0.00	0.00	0.00	6
W_6S_2	C_1	–230.04	–235.65	–234.08	3.90	7.03	7.40	5
W_6S_4	C_1	–222.43	–225.77	–223.87	11.50	16.87	17.60	4
W_6S_5	C_1	–222.87	–224.63	–222.81	11.07	18.01	18.67	4
W_6S_6	C_1	–220.03	–223.58	–221.61	13.90	19.06	19.87	4
W_6S_8	C_s	–209.54	–211.46	–209.35	24.40	31.17	32.13	3
W_6S_{11}	C_s	–208.15	–209.29	–207.03	25.79	33.35	34.45	3
W_6S_{14}	C_1	–205.18	–207.08	–204.95	28.76	35.56	36.52	3

while for Ca^{2+}, still very short distances are calculated in most cases (1.55–2.05 Å). The centers of approximate Gaussian distributions for regular hydrogen bonding distances in Mg^{2+} clusters are considerably shorter (1.50 and 1.70 Å) than for Ca^{2+} clusters (1.65 and 1.75 Å). In contrast, typical H–bonds in pure water microclusters center around 1.97 Å [36, 41, 42]. On the other hand, distances for the 2 donors →1 acceptor bonds do not seem to be affected by the identity of the central cation, both centering around 1.85 Å.

(ii) The considerably wider range of hydrogen bond distances in the microsolvation of Mg^{2+} leads to the first solvation shell being more tightly bound via stronger O–Mg interactions than in O–Ca, leaving in turn labile protons in the first solvation shell; those protons are able to interact in more diverse ways with neighboring water molecules producing a larger variety of hydrogen bond distances in the $[Mg\ (H_2O)_n]^{2+}$ clusters.

(iii) A closer look at Mg^{2+} structures W_3S_5, W_4S_9, W_5S_8, W_5S_{11}, W_5S_{12}, W_6S_{15} reveals total or partial dissociation of water molecules. In those conformations, a proton is transferred from the first to the second solvation shell. To further analyze this dissociation, we present Stern–Limbach plots [50] for Ca^{+2} and Mg^{+2} clusters in (Fig. 6) (the water hexamer case is included for comparison). In these plots q_1 and q_2 quantify the symmetry and the length of the H–bond respectively. Values of q_1 near zero will tell that a proton is equally

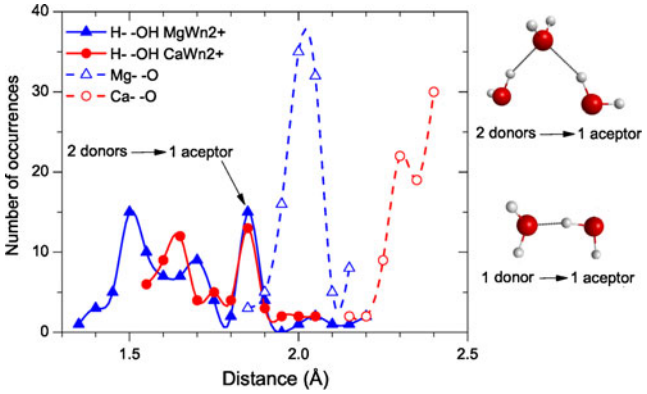

Fig. 5 Distribution of the $H_2O\cdots HOH$ and M–O distances for all $[M(H_2O)_n]^{2+}$ (M=Mg, Ca) clusters considered in this study. At least two types of H–bonds are observed: very short H–bonds (below 1.8 Å) correspond to regular 1 donor → 1 acceptor bonds; longer H–bonds correspond to cases where two H–bonds are donated to the same oxygen atom. Data taken from the MP2/6–311++G** optimized geometries

shared between two oxygen atoms, a precondition for proton transfer. Figure 6 reveals that partial water dissociation is only observed for the $[Mg\ (H_2O)_n]^{2+}$ clusters. Comparison of the three curves shows how the identity of the central cation influences the surrounding hydrogen bond networks. Three distinct types of interactions are clearly seen, with larger deviations from pure water for Mg^{2+}.

Energetics, cluster stabilization and other properties

There are no second or higher order solvation shells among the most stable structures in the microsolvation of Mg^{2+}, Ca^{2+}

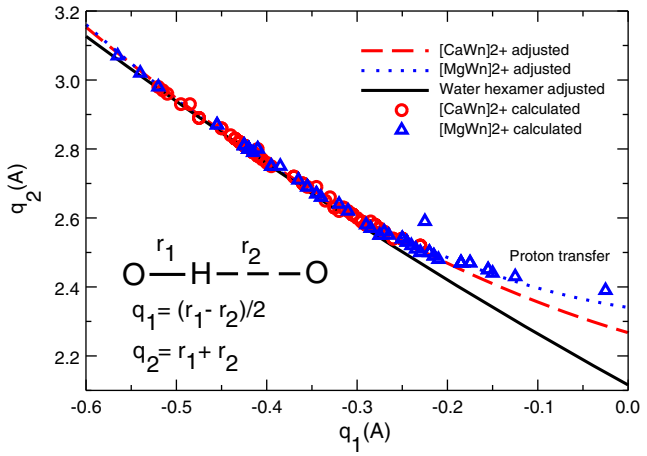

Fig. 6 Stern-Limbach plot: correlation between q_2, the approximate distance between oxygen atoms (exact distance when the three atoms are colinear) and q_1, the approximate distance from the proton to the center of the O···O distance in hydrogen bonding. All systems obey quadratic equations. Partial water dissociation (proton transfer at q_1=0) is only observed for the $[Mg(H_2O)_n]^{2+}$ clusters

(Tables 1 and 2, Figs. 1, 2, 3 and 4). Various types of interactions, mostly electrostatic in nature, drive the stabilization of the arrangements of water molecules in the first solvation shells, while second and higher solvation shells structures and interactions are dictated by comparatively weaker hydrogen bonds subjected to the strong effects of the formal charge in the central cation. We offer evidence to support this claim in our energy decomposition analysis (EDA) below.

Relative binding energies at several levels of theory along with coordination numbers for the central cations for all clusters treated in this study are listed in Tables 1 and 2, from which we draw a number of important observations, all giving additional evidence about the central role electrostatic interactions play in stabilizing the clusters:

(i) Binding energies are very large (≈139–314 kcal mol^{-1} for microsolvation of Mg^{2+}; 104–241 kcal mol^{-1} for Ca^{2+}) when compared to binding energies for Li^+ (62–117 kcal mol^{-1}) [4] and to binding energies for pure water clusters (17–34 kcal mol^{-1} for the trimer to hexamer range) [36, 41, 42, 51]. The larger interaction energies for Mg^{2+} clusters arise from very labile protons (see above).

(ii) There is a direct correlation between the coordination number of the central cation and the stability of the cluster: we observe larger stabilization energies for clusters with larger numbers of direct M···O contacts.

(iii) Large jumps in stabilization energies are obtained by sequentially changing the coordination number of the central cation on a given PES. In contrast, smaller energy variations are observed among isomers with the same coordination. Let us take for example the $[Ca\ (H_2O)_6]^{2+}$ clusters (Table 2), we observe that by reducing the coordination numbers as in the 6 →5 →4 →3 series, energy jumps of 7.40, 10.20, 12.26 kcal mol^{-1} respectively are calculated; on the other hand, the three isomers predicted to have four water molecules around the central cation in the first solvation shell are predicted to be separated by no more than 2.47 kcal mol^{-1}. This observation suggests that the number of water molecules in the first solvation shell, or equivalently, *m*, the coordination number of the central cation, is a good criterion to classify the found structures. We also point out that structures with the same *m* have similar patterns of the hydrogen bond networks.

(iv) The number of H–bonds does not correlate with the stability of the clusters, for example, W_6S_9, having five hydrogen bonds is destabilized with respect to W_6S_1, the most stable isomer for $[Mg\ (H_2O)_6]^{2+}$ (no hydrogen bonds at all) by 37.71 kcal mol^{-1}.

(v) DFT calculated binding energies are in fair agreement with CCSD(T) values for such large systems; MP2 does a better job approximating the CCSD(T) calculations.

(vi) All surfaces have thermodynamically well defined global minima, in the sense that other local minima are considerably higher in energy; in all cases, the global minimum coordinates all water molecules directly to the central cation. This is a strong indication of the dominance of electrostatic contributions over hydrogen bonding in dictating cluster stability in the microsolvation of divalent cations.

Energy decomposition analyses of Mg^{2+} and Ca^{2+} water complexes

We now analyze the driving factors leading to the calculated relative stabilization energies for the studied cation–water complexes. For this purpose, we employ the sequential energy decomposition scheme proposed by Hashimoto and Morokuma [52, 53], where the total binding energy (ΔE_B) is separated into solute–solvent and solvent–solvent contributions. In addition, these contributions are further decomposed into their electrostatic, repulsion, exchange, polarization+charge transfer and dispersion terms to gain better insight into the relationships between the geometrical features of the complexes and the types of interactions driving their formation. This energy decomposition was carried out following the analysis of Su and Li [47] at the full–MP2/6–311++G** level. We have excluded from this analysis those structures containing dissociated water molecules, which will be analyzed in a further section.

In the Hashimoto and Morokuma scheme, cluster total binding energies (ΔE_B) are separated into solvent–solvent interactions, ΔE_S,

$$\Delta E_S = E\left[(\mathrm{H_2O})_n^*\right] - nE[\mathrm{H_2O}], \quad (1)$$

and solute–solvent interactions, ΔE_M,

$$\Delta E_M = E\left[\mathrm{M(H_2O)_n}\right]^{2+} - E\left[\mathrm{M}^{2+}\right] - E\left[(\mathrm{H_2O})_n^*\right]. \quad (2)$$

Here, $E[(H_2O)_n{}^*]$ is the energy of a supermolecule formed by n H_2O molecules fixed at the geometry of the $[M(H_2O)_n]^{2+}$ complex. In this way, ΔE_S gives the interaction energy among the solvent molecules in the complex. ΔE_M is the interaction energy between the prepared solvent supermolecule and the M^{2+} cation. The sum of the two components gives the total binding energy ΔE_B:

$$\Delta E_B = \Delta E_S + \Delta E_M. \quad (3)$$

In this treatment, ΔE_S and ΔE_M can be understood as formation energies. In that case, ΔE_S corresponds to the formation energy of the solvent supermolecule from individual solvent molecules, while ΔE_M is the formation energy of the complex between the solvent supermolecule and the solute.

Tables 3 and 4 list the ΔE_M, ΔE_S and ΔE_B contributions for all the structures studied in this work. As established above, a clear relationship between the coordination number in the first solvation shell (m) and cluster stability emerges. For a given PES, all structures with no dissociated waters for the same m have similar values of ΔE_M, ΔE_S and ΔE_B. ΔE_M is responsible for cluster stabilization (negative sign) while ΔE_S is generally positive and responsible for its destabilization. The positive sign of ΔE_S results from the repulsion between several lone pairs and several bond dipole components of water molecules left to interact once the central cation is removed. In the few negative occurrences of ΔE_S for clusters containing no dissociated water molecules (W_3S_2, W_4S_8, W_5S_9, W_5S_{10}, W_5S_{13}, all for Ca^{2+} complexes), it is clear that after removing the Ca^{2+}, the resulting arrangement of solvent molecules has a stabilizing hydrogen bond network that compensates for the repulsive interactions left at relatively long distances. Figure 7 presents trends on these terms for $[M(H_2O)_6]^{2+}$ clusters as a function of m. Solute–solvent interaction ΔE_M trends for Mg^{2+} and Ca^{2+} cations are very similar, decreasing asymptotically (becoming more negative) as m increases. Similarly, solvent–solvent interaction ΔE_S trends for these cations present the same behavior, becoming more positive as m increases.

The above trends, analogous to those reported for the microsolvation of the Li^+ cation [4], clearly show that solute–solvent interactions are dominant in stabilizing the clusters. In order to unveil the origin of the trends in ΔE_S and ΔE_M as a function of m and to understand the differences between Mg^{2+} and Ca^{2+} hydration, we performed energy decomposition analyses of these terms following the EDA scheme proposed by Su and Li [47]. In this scheme, the interaction energy of any number of monomers is split into five terms: electrostatic (ΔE^{ele}), exchange (ΔE^{exc}), repulsion (ΔE^{rep}), polarization + charge transfer (ΔE^{pol+ct}) and dispersion (ΔE^{dis}). The latter term is equal to the post Hartree–Fock correction to the interaction energy (applicable in our case to MP2 calculations).

Our EDAs on ΔE_M for structures containing no dissociated water molecules considered two monomers: the M^{2+} cation and the water supermolecule $[(H_2O)_n^*]$ at its fixed geometry in the $[M(H_2O)_n]^{2+}$ complex. As listed in Tables 5 and 6, ΔE_M^{ele}, ΔE_M^{exc} and ΔE_M^{pol+ct} (always negative in sign) are responsible for the stabilization of the complexes, whereas ΔE_M^{rep} and ΔE_M^{dis} (always positive in sign) are destabilizing factors. Notice that Mg^{2+} stabilization terms are larger in magnitude (more negative) than those for Ca^{2+}. For instance, ΔE_M^{pol+ct} and ΔE_M^{ele} are about 20 and 40 % larger for Mg^{2+}. Conversely, the sum of destabilization contributions to ΔE_M are larger (more positive) in Ca^{2+} than in Mg^{2+}. Inspecting the magnitudes of the stabilizing terms for the $[Mg(H_2O)_n]^{2+}$ clusters, we find that ΔE_M^{pol+ct} is in all cases at least four times larger than ΔE_M^{exc} and about half of ΔE_M^{ele}, which represent around 30 % of the total stabilization contributions to ΔE_M in

Table 3 Energy decomposition for $[Mg(H_2O)_n]^{2+}$ systems. Total ΔE_B, solute–solvent ΔE_M and solvent–solvent electronic contributions calculated at the MP2/6–311++G** level of theory. *m* is the coordination number of the central cation

Structure	ΔE_M	ΔE_S	ΔE_B	*m*
$[Mg(H_2O)_3]^{2+}$				
W_3S_1	–205.56	5.93	–199.63	3
W_3S_3	–187.42	6.36	–181.06	2
W_3S_5*	–194.23	–141.34	–335.57	1
W_3S_6	–150.92	7.19	–143.73	1
$[Mg(H_2O)_4]^{2+}$				
W_4S_1	–255.87	12.34	–243.53	4
W_4S_3	–233.22	5.10	–228.12	3
W_4S_4	–238.40	9.68	–228.72	3
W_4S_6	–222.25	9.93	–212.32	2
W_4S_7	–212.04	8.38	–203.66	2
W_4S_9[a]	–246.00	–146.67	–392.67	2
W_4S_{10}	–170.68	7.09	–163.59	1
$[Mg(H_2O)_5]^{2+}$				
W_5S_1	–294.20	20.66	–273.54	5
W_5S_2	–281.78	11.98	–269.80	4
W_5S_3	–265.05	9.03	–256.02	3
W_5S_5	–268.22	13.16	–255.06	3
W_5S_6	–265.05	9.07	–255.98	3
W_5S_7	–262.85	9.05	–253.80	3
W_5S_8[a]	–269.48	8.54	–260.94	3
W_5S_{11}[a]	–274.13	–192.40	–466.53	2
W_5S_{13}	–185.22	3.04	–182.18	1
$[Mg(H_2O)_6]^{2+}$				
W_6S_1	–329.51	28.70	–300.81	6
W_6S_2	–319.62	21.56	–298.06	5
W_6S_3	–307.50	12.24	–295.26	4
W_6S_4	–308.92	15.55	–293.37	4
W_6S_5	–306.78	15.13	–291.65	4
W_6S_6	–309.62	18.74	–290.88	4
W_6S_7	–298.68	9.61	–289.07	4
W_6S_8	–291.83	12.24	–279.59	3
W_6S_9	–287.39	8.82	–278.57	3
W_6S_{10}	–289.76	11.75	–278.01	3
W_6S_{11}	–282.44	6.65	–275.79	3
W_6S_{12}	–282.52	6.70	–275.82	3
W_6S_{13}	–281.52	7.39	–274.13	3
W_6S_{14}	–279.00	6.28	–272.72	3
W_6S_{15}[a]	–309.34	–178.03	–487.37	3

[a] Structure with one dissociated water molecule

Table 4 Energy decomposition for $[Ca(H_2O)_n]^{2+}$ systems. Total ΔE_B, solute–solvent ΔE_M and solvent–solvent ΔE_S contributions calculated at the MP2/6–311++G** level of theory. *m* is the coordination number of the central cation

Structure	ΔE_M	ΔE_S	ΔE_B	*m*
$[Ca(H_2O)_3]^{2+}$				
W_3S_1	–147.77	4.09	–143.68	3
W_3S_2	–128.05	–0.47	–128.5	2
W_3S_4	–130.82	2.57	–128.25	2
W_3S_6	–109.82	2.48	–107.34	1
$[Ca(H_2O)_4]^{2+}$				
W_4S_1	–188.94	8.67	–180.27	4
W_4S_2	–186.89	9.05	–177.84	4
W_4S_3	–171.08	2.17	–168.91	3
W_4S_4	–173.03	5.40	–167.63	3
W_4S_5	–156.86	3.47	–153.39	2
W_4S_6	–155.98	2.95	–153.03	2
W_4S_7	–152.24	3.27	–148.97	2
W_4S_8	–145.24	–3.71	–148.95	2
W_4S_{10}	–124.54	0.59	–123.95	1
$[Ca(H_2O)_5]^{2+}$				
W_5S_1	–224.04	14.33	–209.71	5
W_5S_2	–210.98	7.23	–203.75	4
W_5S_3	–195.33	3.35	–191.98	3
W_5S_4	–192.36	0.97	–191.39	3
W_5S_7	–196.48	6.46	–190.02	3
W_5S_5	–194.05	3.73	–190.32	3
W_5S_9	–187.04	–0.99	–188.03	3
W_5S_{10}	–168.43	–2.13	–170.56	2
W_5S_{13}	–135.51	–4.12	–139.63	1
$[Ca(H_2O)_6]^{2+}$				
W_6S_1	–255.84	20.51	–235.33	6
W_6S_2	–245.65	13.63	–232.02	5
W_6S_4	–233.10	8.75	–224.35	4
W_6S_5	–231.82	8.91	–222.91	4
W_6S_6	–233.48	11.58	–221.90	4
W_6S_8	–216.89	4.76	–212.13	4
W_6S_{11}	–210.10	0.10	–210.00	3
W_6S_{14}	–208.20	0.63	–207.57	3

[a] Structure with one dissociated water molecule

Mg^{2+} complexes. This is an important difference with monovalent cations, such as Li^+, where the polarization and charge transfer terms turn out to be very small when compared to the electrostatic and exchange ones [4]. For Ca^{2+}, the polarization term is not as important as in the case of Mg^{2+}, representing 21 % of the total stabilization contributions to ΔE_M in average. On the other hand, ΔE_M^{dis} and ΔE_M^{rep}, the destabilizing terms, follow similar trends for both cations, remaining almost constant as a function of *m*.

We find that ΔE_M^{exc} remains almost constant as a function of *m*, for both, Mg^{2+} and Ca^{2+} complexes, thus, differences between these two cations are mainly due to the behavior of ΔE_M^{ele} and ΔE_M^{pol+ct}. Figure 8 plots the values of EDA decomposition terms for ΔE_M in $[M(H_2O)_6]^{2+}$ clusters. It is clearly seen that for Mg^{2+},

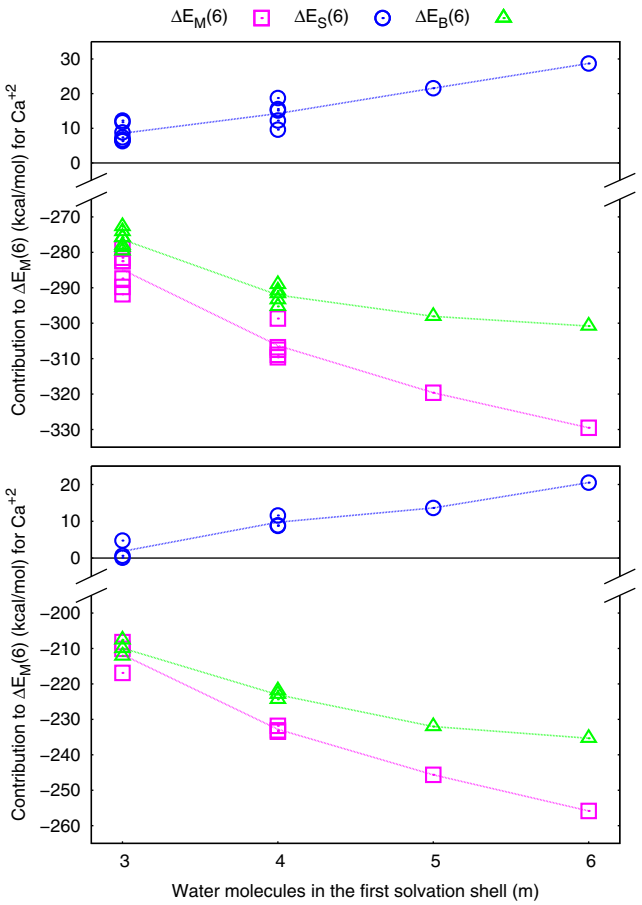

Fig. 7 Hashimoto and Morokuma energy decomposition analysis for all $[M(H_2O)_6]^{2+}$ clusters: ΔE_S, ΔE_M and ΔE_B as a function of m, the number of water molecules in the first solvation shell. Trend lines correspond to averaged values calculated for each contribution. Structures with dissociated waters are not considered

ΔE_M^{ele} remains constant for $m \geq 4$ and that the changes in ΔE_M^{pol+ct} are responsible for the trend of ΔE_M as a function of m. Therefore, in this case, polarization and charge transfer are the factors leading to preferred six–coordinated cations. On the other hand, for Ca^{2+}, both ΔE_M^{ele} and ΔE_M^{pol+ct}, decrease as m increases. The decreasing values of ΔE_M^{ele} and ΔE_M^{pol+ct} for Ca^{2+} clusters is a consequence of the larger O···Ca distances when compared to O···Mg separations (Fig. 5), given that polarization and charge transfer effects become important at shorter internuclear distances. For Ca^{2+}, ΔE_M is almost equal to ΔE_M^{ele}, which suggests that explaining interactions of Ca^{2+} and water molecules only in terms of electrostatic forces would be enough to understand its hydration, unlike Mg^{2+}, where polarization and charge transfer effects have to be taken into account.

In order to gain a better understanding of the interactions involved in forming the water supermolecules, we have performed EDAs for ΔE_S. Here, each water molecule was considered as a monomer and the $[(H_2O)_n^*]$ complex as the supermolecule. The results of our analyses, summarized in Tables 7 and 8 are very similar to those obtained in the case of lithium hydration [4], showing that ΔE_S^{exc}, ΔE_S^{pol+ct} and ΔE_S^{dis} are responsible for the stabilization of the complexes whereas ΔE_S^{rep} is a destabilizing interaction. ΔE_S^{ele} can act as either a stabilizing or destabilizing term depending on the disposition of the water molecules, when a set of hydrogen bonds could

Table 5 EDA decomposition of solute–solvent interactions in $[Mg(H_2O)_n]^{2+}$ systems at the MP2/6–311++G** level. Electrostatic ΔE_M^{ele}, exchange ΔE_M^{exc}, repulsion ΔE_M^{rep}, polarization and charge transfer ΔE_M^{pol+ct} and dispersion ΔE_M^{dis} contributions. All energies in kcal mol^{-1}

Structure	ΔE_M^{ele}	ΔE_M^{exc}	ΔE_M^{rep}	ΔE_M^{pol+ct}	ΔE_M^{dis}	m
$[Mg(H_2O)_3]^{2+}$						
W_3S_1	–173.52	–22.17	67.48	–86.88	9.53	3
W_3S_3	–167.30	–21.12	64.34	–70.69	7.35	2
W_3S_5[a]	–195.03	–22.22	67.91	–52.19	7.30	1
W_3S_6	–144.97	–17.73	53.95	–46.96	4.78	1
$[Mg(H_2O)_4]^{2+}$						
W_4S_1	–211.54	–24.38	74.17	–106.96	12.85	4
W_4S_3	–200.29	–23.73	72.23	–91.88	10.45	3
W_4S_4	–206.29	–24.29	73.96	–92.29	10.51	3
W_4S_6	–202.09	–23.61	71.93	–76.79	8.30	2
W_4S_7	–192.93	–23.21	70.69	–74.65	8.05	2
W_4S_9[a]	–231.54	–26.32	80.41	–79.04	10.49	2
W_4S_{10}	–165.52	–19.36	58.90	–49.79	5.09	1
$[Mg(H_2O)_5]^{2+}$						
W_5S_1	–235.55	–22.82	69.36	–120.84	15.6	5
W_5S_2	–236.56	–25.48	77.48	–110.95	13.7	4
W_5S_3	–231.88	–25.46	77.52	–96.66	11.43	3
W_5S_5	–235.22	–25.80	78.55	–97.23	11.49	3
W_5S_6	–231.72	–25.51	77.67	–96.93	11.45	3
W_5S_7	–230.29	–25.64	78.08	–96.50	11.50	3
W_5S_8[a]	–238.46	–26.36	80.31	–96.82	11.84	3
W_5S_{11}[a]	–258.08	–27.78	84.81	–84.34	11.25	2
W_5S_{13}	–180.69	–20.52	62.47	–51.72	5.24	1
$[Mg(H_2O)_6]^{2+}$						
W_6S_1	–258.88	–22.19	67.42	–134.57	18.71	6
W_6S_2	–260.10	–23.64	71.85	–124.24	16.52	5
W_6S_3	–261.22	–26.32	80.03	–114.67	14.67	4
W_6S_4	–262.83	–26.59	80.89	–115.14	14.75	4
W_6S_5	–264.05	–26.79	81.49	–115.01	14.74	4
W_6S_6	–252.91	–26.07	79.30	–113.02	14.02	4
W_6S_7	–261.42	–26.74	81.34	–114.68	14.74	4
W_6S_8	–258.71	–27.06	82.39	–100.92	12.46	3
W_6S_9	–254.69	–27.28	83.04	–101.29	12.84	3
W_6S_{10}	–256.10	–26.95	82.06	–101.01	12.25	3
W_6S_{11}	–248.52	–26.14	79.59	–99.08	11.71	3
W_6S_{12}	–248.57	–26.14	79.56	–99.09	11.71	3
W_6S_{13}	–248.78	–26.64	81.11	–99.25	12.03	3
W_6S_{14}	–282.35	–29.35	89.59	–101.52	14.30	3
W_6S_{15}[a]	–246.21	–26.34	80.21	–98.45	11.79	3

[a] Structure with one dissociated water molecule

Table 6 EDA decomposition of solute–solvent interactions in $[M(H_2O)_5]^{2+}$ systems at the MP2/6–311++G** level. Electrostatic ΔE_M^{ele}, exchange ΔE_M^{exc}, repulsion ΔE_M^{rep}, polarization and charge transfer ΔE_M^{pol+ct} and dispersion ΔE_M^{dis} contributions. All energies in kcal mol^{-1}

Structure	ΔE_M^{ele}	ΔE_M^{exc}	ΔE_M^{rep}	ΔE_M^{pol+ct}	ΔE_M^{dis}	m
$[Ca(H_2O)_3]^{2+}$						
W_3S_1	–146.01	–32.67	82.25	–54.08	2.74	3
W_3S_2	–129.20	–29.47	74.11	–45.45	1.95	2
W_3S_4	–133.64	–29.90	75.52	–44.74	1.94	2
W_3S_6	–118.51	–27.59	70.16	–35.20	1.32	1
$[Ca(H_2O)_4]^{2+}$						
W_4S_1	–182.98	–38.48	96.72	–68.23	4.04	4
W_4S_2	–180.05	–36.54	91.75	–66.07	4.02	4
W_4S_3	–170.17	–35.69	89.91	–58.25	3.12	3
W_4S_4	–172.72	–36.22	91.37	–58.59	3.13	3
W_4S_5	–161.45	–33.97	85.95	–49.68	2.29	2
W_4S_6	–160.95	–32.84	83.29	–47.83	2.36	2
W_4S_7	–158.09	–33.00	83.79	–47.39	2.45	2
W_4S_8	–147.17	–31.86	80.22	–48.38	1.96	2
W_4S_{10}	–134.76	–30.37	77.32	–38.09	1.37	1
$[Ca(H_2O)_5]^{2+}$						
W_5S_1	–211.99	–40.99	102.73	–79.42	5.62	5
W_5S_2	–205.45	–40.74	102.44	–71.77	4.55	4
W_5S_3	–195.88	–38.66	97.55	–61.83	3.49	3
W_5S_4	–191.85	–38.40	96.67	–62.48	3.69	3
W_5S_7	–197.02	–38.90	98.24	–62.42	3.62	3
W_5S_5	–195.01	–39.14	98.76	–62.23	3.57	3
W_5S_9	–186.66	–37.44	94.38	–60.41	3.10	3
W_5S_{10}	–172.84	–36.17	91.27	–53.20	2.50	2
W_5S_{13}	–146.96	–32.36	82.50	–40.05	1.35	1
$[Ca(H_2O)_6]^{2+}$						
W_6S_1	–237.97	–43.57	109.03	–90.76	7.43	6
W_6S_2	–234.03	–42.94	107.69	–82.51	6.15	5
W_6S_4	–228.10	–42.88	107.91	–75.07	5.05	4
W_6S_5	–227.39	–43.21	108.77	–75.10	5.12	4
W_6S_6	–228.81	–43.10	108.53	–75.13	5.03	4
W_6S_8	–218.78	–41.50	104.85	–65.50	4.05	3
W_6S_{11}	–210.62	–39.96	100.85	–64.04	3.66	3
W_6S_2	–209.67	–40.65	102.63	–64.21	3.69	3

* Structure with one dissociated water molecule

compensate for the O···O repulsions. Figure 9 illustrates the contributions from all sources to solvent–solvent interactions in all $[M(H_2O)_6]^{2+}$ clusters. This figure clearly reveals that ΔE_S^{exc} and ΔE_S^{pol+ct} terms have similar trends to that for ΔE_S^{rep} but with opposite sign. As a result, these contributions tend to cancel out, leading to a trend in ΔE_S being mainly due to the ΔE_S^{ele} contribution, which changes as the distribution of water molecules in the supermolecules evolves from structures where water dipoles are organized in hydrogen bonded networks, at smaller m

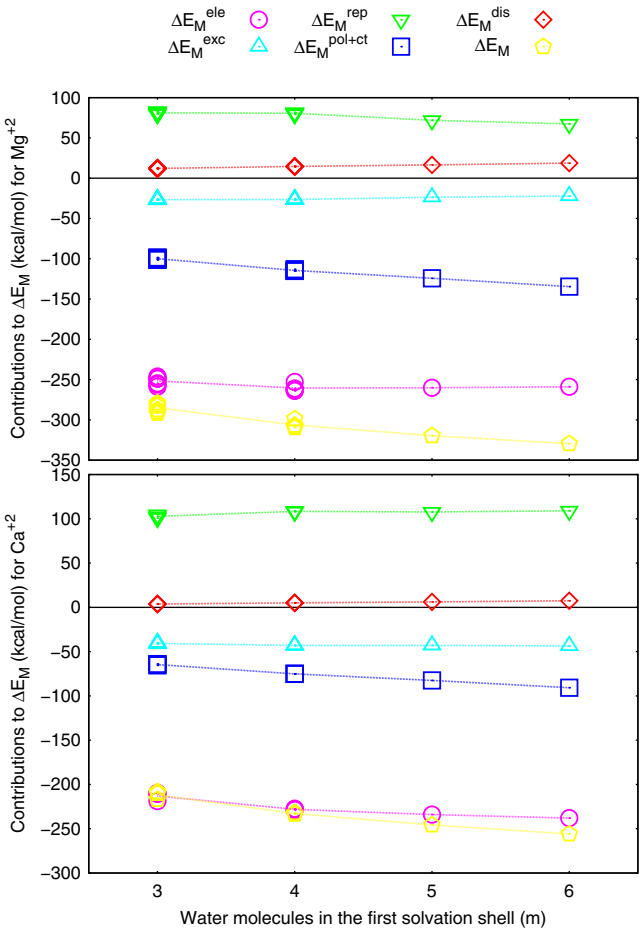

Fig. 8 Su and Li decomposition analysis of solute–solvent interactions calculated for all $[M^{2+}(H_2O)_6]$ clusters: values of electrostatic (ΔE_M^{ele}), exchange (ΔE_M^{exc}), repulsion (ΔE_M^{rep}), polarization+charge transfer (ΔE_M^{pol+ct}) and dispersion (ΔE_M^{dis}) terms as a function of m, the number of water molecules in the first solvation shell. Trend lines correspond to averaged values calculated for each contribution. Structures with dissociated waters are not considered

values, to those when dipoles are placed in very symmetric fashion around the cations, as m increases. In the first case, attractive electrostatic interactions are favored, while in the second case the organization of the dipoles produces repulsive electrostatic interactions. Trends in ΔE_S contributing terms for both cations are similar, however, all interactions have larger magnitudes for Mg^{2+} than for Ca^{2+} clusters, this is a consequence of the differences in the ranges of H···OH distances, which allow for shorter hydrogen bonds in Mg^{2+} (Fig. 5). In conclusion, ΔE_M is the crucial interaction determining differences between hydration of Mg^{2+} and Ca^{2+}.

Structures containing dissociated water molecules

In the previous sections the discussion have focused on the analysis of water–cation clusters where solvent molecules do not experience dissociation. Nonetheless, our calculations

Table 7 EDA decomposition of solvent–solvent interaction in $[Mg(H_2O)_n]^{2+}$ systems at the MP2/6–311++G** level. Electrostatic ΔE_S^{ele}, exchange ΔE_S^{exc}, repulsion ΔE_S^{rep}, polarization and charge transfer ΔE_S^{pol+ct} and dispersion ΔE_S^{dis} contributions. All energies in kcal mol^{-1}

Structure	ΔE_S^{ele}	ΔE_S^{exc}	ΔE_S^{rep}	ΔE_S^{pol+ct}	ΔE_S^{dis}	m
$[Mg(H_2O)_3]^{2+}$						
W_3S_1	7.11	–1.17	1.73	–0.58	–1.15	3
W_3S_3	–23.78	–52.40	102.81	–18.61	–1.65	2
W_3S_5[a]	–139.99	–31.30	59.69	–26.46	–3.27	1
W_3S_6	–40.52	–77.16	150.14	–22.12	–3.16	1
$[Mg(H_2O)_4]^{2+}$						
W_4S_1	–65.55	–120.38	232.12	–34.60	–4.48	4
W_4S_3	15.10	–4.20	6.25	–1.98	–2.82	3
W_4S_4	–9.66	–29.74	54.03	–6.19	–3.34	3
W_4S_6	–12.34	–40.00	77.03	–12.32	–2.69	2
W_4S_7	–44.11	–91.97	179.48	–30.36	–3.12	2
W_4S_9[a]	–146.06	–45.09	87.39	–41.94	0.03	2
W_4S_{10}	–79.44	–178.33	355.80	–118.63	5.56	1
$[Mg(H_2O)_5]^{2+}$						
W_5S_1	22.83	–15.68	24.63	–5.10	–6.02	5
W_5S_2	–0.51	–31.53	56.33	–7.30	–5.01	4
W_5S_3	–27.85	–66.32	124.86	–16.88	–4.79	3
W_5S_5	–28.92	–73.60	141.66	–21.76	–4.22	3
W_5S_6	–28.02	–66.82	125.85	–17.09	–4.85	3
W_5S_7	–24.55	–59.63	112.70	–14.82	–4.65	3
W_5S_8[a]	–46.65	–111.34	219.21	–49.50	–3.19	3
W_5S_{11}[a]	–225.65	–120.80	237.09	–73.11	–9.92	2
W_5S_{13}	–91.00	–162.70	313.41	–50.90	–5.75	1
$[Mg(H_2O)_6]^{2+}$						
W_6S_1	33.33	–26.10	40.51	–9.26	–9.78	6
W_6S_2	9.28	–40.95	71.27	–9.97	–8.07	5
W_6S_3	–14.94	–57.07	103.10	–11.73	–7.13	4
W_6S_4	–15.15	–61.90	114.58	–15.35	–6.63	4
W_6S_5	–12.64	–55.89	103.46	–13.29	–6.52	4
W_6S_6	–14.56	–64.23	121.36	–17.81	–6.01	4
W_6S_7	–21.42	–67.33	124.28	–19.35	–6.57	4
W_6S_8	–40.55	–90.85	172.59	–22.77	–6.18	3
W_6S_9	–35.80	–79.76	148.99	–17.58	–7.02	3
W_6S_{10}	–45.66	–100.58	191.37	–27.19	–6.19	3
W_6S_{11}	–49.08	–102.65	193.78	–29.01	–6.39	3
W_6S_{12}	–49.22	–102.96	194.39	–29.12	–6.39	3
W_6S_{13}	–45.57	–98.95	187.92	–29.73	–6.29	3
W_6S_{14}	–43.96	–91.40	172.61	–24.81	–6.17	3
W_6S_{15}[a]	–246.21	–26.34	80.21	–98.45	11.79	3

[a] Structure with one dissociated water molecule

Table 8 EDA decomposition of solvent–solvent interaction in $[Ca(H_2O)_n]^{2+}$ systems at the MP2/6–311++G** level. Electrostatic ΔE_S^{ele}, exchange ΔE_S^{exc}, repulsion ΔE_S^{rep}, polarization and charge transfer ΔE_S^{pol+ct} and dispersion ΔE_S^{dis} contributions. All energies in kcal mol^{-1}

Structure	ΔE_S^{ele}	ΔE_S^{exc}	ΔE_S^{rep}	ΔE_S^{pol+ct}	ΔE_S^{dis}	m
$[Ca(H_2O)_3]^{2+}$						
W_3S_1	4.85	–0.14	0.20	–0.23	–0.58	3
W_3S_2	–15.80	–28.76	52.52	–6.07	–2.35	2
W_3S_4	–16.37	–32.80	62.93	–9.78	–1.41	2
W_3S_6	–31.93	–56.32	107.89	–14.52	–2.64	1
$[Ca(H_2O)_4]^{2+}$						
W_4S_1	–53.52	–90.96	172.51	–23.54	–3.89	4
W_4S_2	10.68	–0.62	0.89	–0.83	–1.45	4
W_4S_3	10.95	–2.26	3.46	–1.10	–2.00	3
W_4S_4	–11.55	–26.67	48.57	–5.58	–2.60	3
W_4S_5	–10.67	–29.02	55.32	–8.39	–1.84	2
W_4S_6	–32.17	–61.11	116.91	–17.55	–2.61	2
W_4S_7	–32.60	–61.49	117.57	–17.94	–2.60	2
W_4S_8	–26.59	–49.06	93.43	–11.88	–2.64	2
W_4S_{10}	–38.19	–66.44	124.11	–19.37	–3.82	1
$[Ca(H_2O)_5]^{2+}$						
W_5S_1	18.22	–3.40	5.16	–2.32	–3.34	5
W_5S_2	–4.65	–25.91	47.02	–5.81	–3.41	4
W_5S_3	–26.19	–53.54	99.77	–12.92	–3.78	3
W_5S_4	–23.95	–47.68	86.64	–9.26	–4.78	3
W_5S_7	–24.39	–54.36	103.40	–15.12	–3.07	3
W_5S_5	–23.71	–48.63	90.78	–10.91	–3.79	3
W_5S_9	–32.49	–61.57	114.69	–17.63	–3.99	3
W_5S_{10}	–48.81	–84.34	158.53	–22.58	–4.93	2
W_5S_{13}	–75.67	–125.61	238.27	–35.97	–5.13	1
$[Ca(H_2O)_6]^{2+}$						
W_6S_1	27.58	–5.98	8.99	–4.50	–5.58	6
W_6S_2	4.04	–27.39	49.03	–6.90	–5.16	5
W_6S_4	–17.20	–49.91	92.52	–11.97	–4.69	4
W_6S_5	–15.23	–45.58	84.59	–10.22	–4.66	4
W_6S_6	–15.56	–50.24	95.02	–13.62	–4.02	4
W_6S_8	–37.07	–72.93	136.87	–17.14	–4.96	3
W_6S_{11}	–45.76	–85.61	160.33	–23.71	–5.16	3
W_6S_{14}	–41.85	–77.63	145.35	–20.13	–5.12	3

[a] Structure with one dissociated water molecule

show that dissociation of solvent molecules is only found in hydrated Mg^{2+} clusters. In order to analyze these structures, we have separated solute–solvent interaction as we did for non-dissociated structures, following Eq. 2. Therefore, ΔE_M for dissociated structures can be directly compared to the ΔE_M for the non-dissociated ones. It is clearly seen, in Tables 3 and 4, that the presence of an anion in the first solvation shell impacts the magnitude of the ΔE_M term making it comparable to that of the most stable structure in the corresponding PES. A further examination of the ΔE_M terms for all structures containing dissociated waters using the EDA decomposition scheme (Tables 5 and 6), reveals that changes in ΔE_M terms are mainly due to ΔE_M^{ele}, the electrostatic interactions. In all cases, the ΔE_M term is larger than the one calculated for structures with no water dissociation for the same m. This is

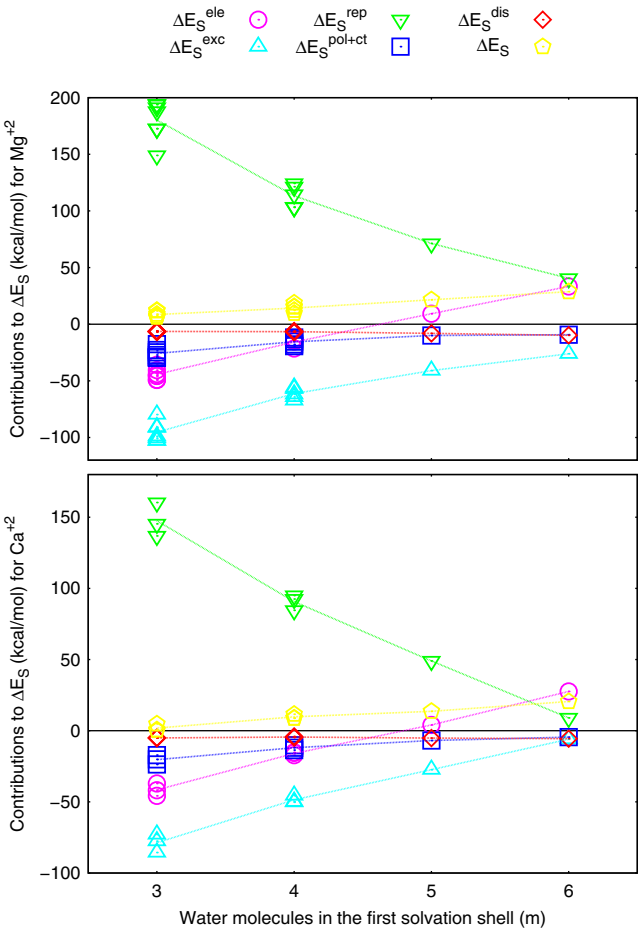

Fig. 9 Su and Li decomposition analysis of solvent–solvent interactions calculated for all $[M^{2+}(H_2O)_6]$ clusters: values of electrostatic (ΔE_M^{ele}), exchange (ΔE_M^{exc}), repulsion (ΔE_M^{rep}), polarization+charge transfer (ΔE_M^{pol+ct}) and dispersion (ΔE_M^{dis}) terms as a function of m, the number of water molecules in the first solvation shell. Trend lines correspond to averaged values calculated for each contribution. Structures with dissociated waters are not considered

a result of the strong attractions between positive and negative charges in Mg^{2+} and hydroxide anions, respectively. This increase in ΔE_M suggests that this particular interaction plays a pivotal role in the Mg^{2+} driven dissociation of water molecules.

We now turn our attention to ΔE_S. To understand changes produced in the solvent structure we separated the system according to the structures of the present ions. For instance, we have split the solvent supermolecule of structure W_3S_5 into two ions: $H_5O_2^+$ and OH^-. Given the different approaches in separating the water supermolecule, a direct comparison of the value of ΔE_S between the dissociated and undissociated cases is not possible. However, the analysis of ΔE_S for the structures containing dissociated waters will provide us with information on the type of interactions at play in the dissociated solvent supermolecule. In this case, as shown in Tables 7 and 8, the electrostatic term ΔE_S^{ele} has the larger contribution to the stabilization energy, given the occurrence of ion–pair interactions not present in a non–dissociated water supermolecule.

The presence or absence of dissociated structures in the PESs of microsolvated cations is an important feature that differentiates Mg^{2+} from Ca^{2+} and from monovalent cations such as Li^+. This particular finding sheds light on the Mg^{2+} capacity to promote the formation of a hydroxide anion in its first solvation shell, which is necessary to regulate proton transfer processes in enzymes with exonuclease activity [12, 13].

Conclusions and perspectives

Sixty six structures were identified in the $[Mg(H_2O)_n)]^{+2}$, $[Ca(H_2O)_n)]^{+2}$ (n=3, 4, 5, 6) potential energy surfaces explored using the ASCEC method. The structures were produced at the B3LYP/6–31G* and MP2/6–311++G** levels after optimizing and characterizing candidate structures generated by random walks of the HF/6–31G* conformational spaces. A direct correlation between the coordination number of the central cation and cluster stability is found. Dissociation of water molecules in the first solvation shell is predicted as a consequence of the presence of the strong formal charges in Mg^{2+} clusters; this dissociation produces a hydroxide anion which strongly binds to the central cation, while the remaining proton is transferred to outer solvation shells where a Zundel type cation is produced via a Grotthus mechanism. Two types of H–bonds were identified: regular 1 donor → 1 acceptor and 2 donors → 1 acceptor. Distribution of H–bond distances suggests that very labile protons in Mg^{2+} clusters favor the formation of unusually short 1 donor → 1 acceptor H–bonds and largely disturbs the hydrogen bonding networks in outer solvation shells. The 2 donors → 1 acceptor H–bonds do not seem to be affected by the identity of the central cation. Our decomposition energy analysis of the non–dissociated water complexes shows that the polarization and charge transfer contributions to solute–solvent interactions are crucial to explain total energy trends and stability in Mg^{2+} water complexes. In contrast, the same term is not as significant for Ca^{+2}, where the electrostatic term dominates. The decomposition energy analysis of dissociated structures in Mg^{2+} PESs suggests that their formation is favored by the strong electrostatic interaction between the hydroxide and Mg^{2+} ions.

Acknowledgments Partial financial support for this work was provided by Colciencias (grant CT 457–2009); The Research Office of University of Medellín, project 626, and Comite para el desarrollo de la investigacion (CODI) office, Universidad de Antioquia.

References

1. Furukawa K, Ohashi K, Koga N, Imamura T, Judai K, Nishi N, Sekiya H (2011) Chem Phys Lett 508:202
2. Neff D, Simmons J (2008) Int J Mass Spectrom 277:166
3. Lei X, Pan BJ (2010) Phys Chem A 114:7595

4. Romero J, Reyes A, David J, Restrepo A (2011) Phys Chem Chem Phys 13:15264
5. Miller D, Lisy JJ (2008) Am Chem Soc 130:15381
6. Miller D, Lisy JJ (2008) Am Chem Soc 130:15393
7. da Silva F, Williams R (1991) The biological chemistry of the elements. Clarendon, Oxford
8. Cowan JA (1995) Biological chemistry of magnesium. VCH, New York
9. Cowan JA (1998) Inorg Chim Acta 275:24
10. Cowan JA (2002) BioMetals 15:225
11. Sigel RKO, Pyle AM (2007) Chem Rev 107:97
12. Boero M, Terakura K, Tateno MJ (2002) Am Chem Soc 124:8949
13. Boero M, Tateno M, Terakura K, Oshiyama AJ (2005) Chem Theory Comput 1:925
14. Ho M, Vivo M, Peraro M, Klein MLJ (2010) Am Chem Soc 132:13702
15. Park JM, Boero MJ (2010) Phys Chem B 114:11102
16. Rodriguez-Cruz S, Jockusch R, Williams RJ (1999) Am Chem Soc 121:8898
17. Rao J, Dinadayalane T, Leszczynski J, Sastry GJ (2008) Phys Chem A 112:12944
18. Pye C, Rudolph WJ (1998) Phys Chem A 102:9933
19. Carl D, Moision R, Armentrout P (2007) Int J Mass Spectrom 265:308
20. Glendening ED, Feller DJ (1996) Phys Chem 100:4790
21. Merrill GN, Webb SP, Donald BBJ (2003) Phys Chem A 107:386
22. Caminiti R, Licheri G, Piccauga G, Pinna G (1977) Chem Phys Lett 47:275
23. Megyes T, Grósz T, Radnai T, Bakó I, Pálinkás GJ (2004) Phys Chem A 108:7261
24. Jalilehvand F, Spangberg D, Lindqvist-Reis P, Hermansson K, Persson I, Sandström M (2000) J Am Chem Soc 123:431
25. Fulton G, Heald S, Badyal Y, Simonson JJ (2003) Phys Chem A 107:4688
26. Bush M, Saykally R, Williams E (2007) Chem Phys Chem 8:2245
27. Lightstone F, Schwegler E, Hood R, Gygi F, Galli G (2001) Chem Phys Lett 343:549
28. Markham G, Glusker J, Bock CJ (2002) Phys Chem B 106:5118
29. Naor M, Nostrand K, Dellago C (2003) Chem Phys Lett 369:159
30. Tongraar A, Liedl K, Rode BJ (1997) Phys Chem A 101:6299
31. Schewnk C, Loeffler H, Rode BJ (2001) Chem Phys 115:10808
32. Pavlov M, Siegbahn P, Sandström MJ (1998) Phys Chem A 102:219
33. Buckingham A, Bene J, McDowell S (2008) Chem Phys Lett 463:1
34. Rao J, Zipse H, Sastry GJ (2009) Phys Chem B 113:7225
35. Neela J, Mahadevi A, Sastry GJ (2010) Phys Chem B 114:17162
36. Pérez J, Hadad C, Restrepo A (2008) Int J Quantum Chem 108:1653
37. Pérez J, Flórez E, Hadad C, Fuentealba P, Restrepo AJ (2008) Phys Chem A 112:5749
38. Pérez J, Restrepo A (2008) ASCEC V–02: Annealing Simulado con Energía Cuántica. Property, development and implementation: Grupo de Química–Física Teórica, Instituto de Química, Universidad de Antioquia: Medellín, Colombia
39. David J, Guerra D, Hadad C, Restrepo AJ (2010) Phys Chem A 114:10726
40. Yepes D, Kirk S, Jenkins S, Restrepo A (2012) J Mol Mod 18:4171
41. Ramírez F, Hadad C, Guerra D, David J, Restrepo A (2011) Chem Phys Lett 507:229
42. Hincapié G, Acelas N, Castaño M, David J, Restrepo AJ (2010) Phys Chem A 114:7809
43. Jenkins S, Restrepo A, David J, Yin D, Kirk S (2011) Phys Chem Chem Phys 13:11644
44. Murillo J, David J, Restrepo A (2010) Phys Chem Chem Phys 12:10963
45. David J, Guerra D, Restrepo AJ (2009) Phys Chem A 113:10167
46. Frisch MJ, Trucks GW, Schlegel HB, Scuseria GE, Robb MA, Cheeseman JR, Montgomery JA, Vreven T Jr, Kudin KN, Burant JC, Millam JM, Iyengar SS, Tomasi J, Barone V, Mennucci B, Cossi M, Scalmani G, Rega N, Petersson GA, Nakatsuji H, Hada M, Ehara M, Toyota K, Fukuda R, Hasegawa J, Ishida M, Nakajima T, Honda Y, Kitao O, Nakai H, Klene M, Li X, Knox JE, Hratchian HP, Cross JB, Bakken V, Adamo C, Jaramillo J, Gomperts R, Stratmann RE, Yazyev O, Austin AJ, Cammi R, Pomelli C, Ochterski JW, Ayala PY, Morokuma K, Voth GA, Salvador P, Dannenberg JJ, Zakrzewski VG, Dapprich S, Daniels AD, Strain MC, Farkas O, Malick DK, Rabuck AD, Raghavachari K, Foresman JB, Ortiz JV, Cui Q, Baboul AG, Clifford S, Cioslowski J, Stefanov BB, Liu G, Liashenko A, Piskorz P, Komaromi I, Martin RL, Fox DJ, Keith T, Al-Laham MA, Peng CY, Nanayakkara A, Challacombe M, Gill PMW, Johnson B, Chen W, Wong MW, Gonzalez C, Pople JA (2004) Gaussian 03, Revision E.01. Gaussian Inc, Wallingford
47. Su P, Li HJ (2009) Chem Phys 131:014102
48. Schmidt MW, Baldridge KK, Boatz JA, Elbert ST, Gordon MS, Jensen JH, Koseki S, Matsunaga N, Nguyen KA, Su SJ, Windus TL, Dupuis M, Montgomery JA (1993) J Comput Chem 14:1347
49. de Grotthus C (1806) Ann Chim 58:54
50. Limbach H, Tolstoy P, Pérez-Hernández N, Gou J, Shemderovich J, Denisvo G (2009) Isr J Chem 49:199
51. Taketsugu T, Wales D (2002) Mol Phys 100:2793
52. Hashimoto K, Morokuma KJ (1994) Am Chem Soc 116:11436
53. Hashimoto K, Kamimoto TJ (1998) Am Chem Soc 120:3560